Integrative Biology

Accepted Manuscript

ROYAL SOCIETY OF CHEMISTRY

www.rsc.org/ibiology

Insight, innovation, integration

Emerging evidence surggests that nervous systems contribute to tumor growth and progression. However, few *in vitro* models are suitable for investigating their interaction. Here, we reported the use of a microfluidic compartmentalized device to simulate the interaction between neurons and cancer cells. We demonstrated that nerves provided biophysical support for cancer cells and guided their directional migration, which was consistent with clinical metastatic behaviors of different types of cancers. Our on-chip model provided a useful platform to investigate the roles of nerves on cancer progression, and can broaden the chemical space in screening neuronal drugs for cancers.

Journal Name

ARTICLE

An on-chip model for investigating the interaction between neurons and cancer cells

Received 00th January 20xx,
Accepted 00th January 20xx

DOI: 10.1039/x0xx00000x

www.rsc.org/

Yifeng Lei,[a] Jun Li,[a] Nuoxin Wang,[a] Xinglong Yang,[a] Yoh Hamada,[b] Qizhai Li,[c] Wenfu Zheng*[a] and Xingyu Jiang*[a]

Emerging evidence suggests that there is extensive interaction between neurons and cancer cells. However, few model systems have been developed to investigate nerve-cancer interaction *in vitro*. Herein, a high-throughput microfluidic compartmentalized chip is developted to examine the interaction between neurons and cancer cells. The nerve bundles appear to provide biophysical support for cancer cells and guide their directional migration. The cancers that have high levels of perineural invasion in clinical observations exhibit greater migration along neurites in the on-chip model. The on-chip model allows the screening of compounds which inhibit cancer cell migration along neurites *in vitro*. The interruption of neurites, the pharmacological blockade of nerve-cancer signaling, effectively attenuate the migration of cancer cells along neurites. This on-chip model provides a useful platform to investigate the dynamic interaction between cancers and neurons, and can dramatically broaden the chemical space in screening neuron-related drugs for cancers.

Introduction

Emerging studies suggest that the neural microenvironment is a novel niche in cancer growth and progression. In fact, this topic has been received increased attention recently.[1-5] The neural microenvironment plays a critical role in cancer progression,[6] for example, the cancer cells can migrate and spread along nerves, a process termed perineural invasion (PNI), which is an important pathologic feature and correlates with poor prognosis and decreased survival in certain cancers.[7-10] Increasing evidence suggests reciprocal interaction between cancer and nerves. Cancer cells secrete neurotrophic factors and axon guidance molecules to stimulate the neurite growth in solid tumors.[11, 12] In turn, nerves secrete chemokines and neurotransmitters which generate a positive microenvironment for survival, proliferation and metastasis of cancers.[11, 12]

Modeling the effect of nerves on cancer progression may provide novel insights in understanding the neurosignaling in cancer and help the development of anti-cancer therapy. However, to date, research towards studying nerve-cancer crosstalk has been largely hampered due to lack of a robust, and biologically relevant, in-vitro model/ system.[7] Animal models have been the foundation of cancer research. For instance, gene knockout mice were generated to study the contribution of automonic nerves on prostate cancer progression,[1] and *in vivo* chick chorioallantoic membrane (CAM) model was developed to investigate tumor invasion and metastasis in head and neck cancer.[3] However, animal models are generally limited due to high cost and long experiments. The development of robust and effective *in vitro* neuron-cancer models that accurately mimic the *in vivo* tumor microenvironment is important for advancing the knowledge of cancer biology and for developing rapid, high-throughput screening in drug development and testing.

Compared to traditional *in vitro* cell culture techniques,[13] microfluidic systems offer great opportunities for the spatial-temporal control of cells and cellular microenvironments due to their microscale precision and high-throughput capability.[14-19] More specifically, Taylor et al. developed the microfluidic compartmentalized chips for neuron culture, in which neuron somas and neurites can be separated in different compartments.[20] Benefiting from this culture platform, we are able to advance our knowledge in neuroscience and neurobiology previously.[21-25]

In this work, we present a high-throughput microfluidic compartmentalized chip to study the nerve-cancer interaction *in vitro*. In particular, we aim to study the migration of cancer cells associated with neurites, in order to mimic the process of perineural invasion of cancers *in vivo*. Our results show that the neurites provide biophysical supports for cancer cell attachment and guide their directional migration. The cancers that have high rate of perineural invasion in clinical observations exhibit greater migration along neurites in the on-chip model. Further, we apply this on-chip model to screen

a Beijing Engineering Research Center for BioNanotechnology, CAS Key Laboratory for Biological Effects of Nanomaterials and Nanosafety, National Center for NanoScience and Technology, Beijing100190, China. Email: xingyujiang@nanoctr.cn; zhengwf@nanoctr.cn
b Department of Nano-Medical Science, Graduate School of Medicine, Tohoku University, Sendai 980-8575, Japan.
c Academy of Mathematics and Systems Science, Chinese Academy of Sciences, Beijing 100190, China.
† Electronic Supplementary Information (ESI) available. See
DOI: 10.1039/x0xx00000x

the compounds for the inhibition of cancer cell migration along neurites. We demonstrate that the inhibition of signaling between neuronal and cancer cells impairs the migration of said cancer cells along the paths of outgrown neurites. This suggests a possible application of our on-chip model towards the investigation of the roles nerves play in tumor progression.

Materials and methods

Microfluidic chip fabrication

We fabricated microfluidic compartmentalized devices using standard soft lithography and replica molding.[17, 26] Briefly, we used photolithography to pattern two layers of negative photoresist, SU-8 (MicroChem., MA, US), onto a silicon wafer, resulting in a master with positive relief patterns of cell culture compartments and microgrooves. We cast and cured a pre-polymer mixture of Sylgard® 184 at 10:1 ratio (Dow Corning) against the positive relief master to obtain a negative replica-molded piece. After curing, we peeled off the PDMS from the master and punched inlets and outlets of the channels with a sharpened needle. We sterilized the PDMS devices at 121 °C and 15 psi for 15 min. We cleaned the cell culture dishes (35mm x 10mm, Corning) with purified water and coated them with 0.1 mg/mL poly-D-lysine (PDL, Sigma) for overnight before use. We sealed the PDMS pieces to PDL-coated dishes by conformal contact to form the enclosed channels (Fig. 1A). This type of reversible contact resulted in both a water-tight seal during use and the easy release of the PDMS pieces from the substrates as desired.

Cell preparation

The cell preparation and culture was performed in accordance with approved guidelines of the Institutional Animal Care and Use Committee at National Center for Nanoscience and Technology (ACUC-NCNST, IRB Number 2013-0016). We prepared hippocampal and cortical neurons from embryonic SD rats (E18) as described previously.[17, 26, 27] We isolated dorsal root ganglion (DRG) neurons from postnatal SD rats (weight ~ 60 g) according to previously established techniques.[28] We suspended the hippocampal, cortical or DRG neurons into a density of approximate 6×10^7 cells/mL in neuron culture medium (Neurobasal® medium containing 2% B27 supplements and 1% penicillin streptomycin (PS)) for use.

The human cancer cell lines, including prostate cancer cell line PC-3, pancreatic cancer cell line Panc-1 and breast cancer cell line MCF-7, were obtained from Institute of Basic Medical Sciences, Chinese Academy of Medical Sciences. The selection of cancer cell lines was based on the clinical observation of different rate of perineural invasion of cancers.[9] PC-3 cells were maintained in F12K medium supplemented with 10% fetal bovine serum (FBS), and 1% PS. MCF-7 and Panc-1 cells were maintained in DMEM medium with 10% FBS and 1% PS. PC-3 cells transfected with luciferase gene (PC-3-luc cells) were obtained from Institute of Laboratory Animal Sciences (ILAS), CAMS & PUMS, and maintained in DMEM/F12 supplemented with 10% FBS, 1% PS and 500 μg/ml G418. All cancer cell lines were routinely maintained and passaged in a humidified atmosphere containing5% CO_2 at 37 °C.

Cell culture in microfluidic devices

We first introduced approximately 10 μl neuron suspension into the left channel of the microfluidic device, and filled the right channel with neuron culture medium. The entire chamber were immersed in neuron culture medium during culture. After 4-5 days, the neurites extended to cross the interconnected microgrooves. We carefully removed the medium outside of the chambers and in the right channel, and introduced the cancer cells at density of approximate 6×10^6 cells/mL into the right channels, then we immersed the device in neuron culture medium for incubation. We let the cancer cells adhere for 6 h, and then we removed the medium outside of the chambers, and carefully removed the cover by peeling the PDMS from the neuronal side to cancer sides. We washed away the non-adhered cells and debris, and observed the neuro-cancer cell interactions by microscopy. The neuron-cancer co-cultures were maintained in neuron culture medium.

Chemical or physical ablation of neurites

To induce neuron injury, we introduced 6-hydroxydopamine (6-OHDA, 100 μM) in the neuronal compartment for 1 h to induce acute neuron injury. We peeled off the PDMS cover to observe the nerve-cancer interaction as described above. Otherwise, we carried out the neuron-cancer co-culture as described in previous section. After peeling off the PDMS covers, we carefully removed the neurites in the interconnected regions by tweezers under a stereomicroscope (Leica). We washed away the cell debris, and investigated the migration of cancer cells as described above.

Blocking of surface receptors on cancer cells

We incubated the PC-3 cells with β-blockers (propranolol and penbutolol) (10 μM for each), muscarinic antagonists (atropine and hyoscine) (10 μM for each) in the cell culture medium overnight, we then seeded the pre-treated PC-3 cells into microfluidic devices as previously described. PC-3 cells without drug treatments served as controls.

Video recording

We used time-lapse video to record the cancer cell migration. We transferred the cell culture dishes onto the motorized stage of time-lapse microscopy enclosed in a humidified atmosphere at 37 °C and 5% CO_2 (Leica DMI 6000B). We recorded the images of cells every 5 minutes for up to 24 hours to follow the cancer cell locomotion. We analyzed the videos using Time Lapse Analyser and ImageJ software as previously described.[29] We plotted the centroids of individual cancer cells at intervals of 3 hours to illustrate different modes of cancer cell migration.

Immunofluorescence of on-chip cells

We fixed the cells using 4% paraformaldehyde (PFA) for 15 min at room temperature, permeabilized with 0.3% Triton X-100 and blocked with 1% bovine serum albumin (BSA). We

incubated the samples with primary antibodies at 4 °C overnight. The primary antibodies are: mouse monoclonal to III Tubulin (Tuj1, Abcam), rabbit polyclonal to pan-cytokeratin (panCK, Abcam). We incubated the samples with secondary antibodies conjugated with AlexaFluo® 488 or 568 (Invitrogen) for 1 h at 37 °C. We counterstained the cell nuclei using DAPI (Invitrogen) for 10 minutes, mounted the cells with Prolong® Gold antifade reagent (Invitrogen) and observed with confocal microscopy (Carl Zeiss LSM710).

Statistical analysis

All *in vitro* experiments based on at least five independent repeats for each condition, and three repetitions of the experiments. Data were displayed as mean value ± standard deviation (sd). Statistical analysis was performed using Student's t-test. $P<0.05$ was considered as statistically significant.

Results

Microfluidic compartmentalized chip design

We developed a high-throughput microfluidic compartmentalized chip to investigate the *in vitro* neuron-cancer interaction. The microfluidic device contained two separate compartments (2 mm wide, 150 µm high, 2 cm long), which were connected by 1000 parallel ultraminiaturized microchannels (5 µm wide, 5 µm high, 450 µm long) (Fig. 1A). The microfluidic chips were adapted to fit into 6-well cell culture plate. Neurons and cancer cells can be separately seeded into the main compartments (Fig. 1A-C). The neuronal cell bodies (soma) and cancer cells were limited to the main channels, whereas only the neurites can grow and cross the interconnected, ultraminiaturized microchannels (5 µm wide, 5 µm high). We seeded the dissociated DRG neurons into the neuronal compartment. As expected, the neurites crossed the interconnected microchannels and were readily detected in the opposite compartment by day *in vitro* 4 (DIV 4) (Fig. 1B, D-E, G-H). Due to the limited space of interconnected microchannels, the neuronal soma and cancer cells were limited in the main channels, respectively (Fig. 1B, C).

Neurites facilitate the migration of cancer cells

We investigated the migration of cancer cells associated with neurites using the above device. We first cultured DRG neurons in the neuronal compartment. When the neurites extended to the opposite channel at DIV4, we seeded the prostate cancer PC-3 cells in the opposite compartment. We let the PC-3 cells adhere for 6 h and carefully peeled off the PDMS cover from the substrates, to investigate the nerve-cancer interaction (Fig. S1A). The devices without interconnected microgrooves, namely, no neurites in the interconnected regions served as controls (Fig. S1B). The presence of neurites accelerated the migration of the PC-3 cells as compared to the controls without the presence of neurites in the interconnected regions (Fig. 2A-B). Magnified phase-contrast images and fluorescent images showed that the PC-3 cells navigated along the neurites (Fig. 2C, E-F). The quantification of the surface area covered by the migrated PC-3 cells in the interconnected regions showed that the migration of PC-3 cells along neurites consistently occurred and increased over time (Fig. 2D).

We disrupted the neurites in the on-chip platform to reveal the effects that neurites play on the migration of cancer cells (Fig. S2). After physical removal of the neurites in the interconnected regions by tweezers, the migration of the PC-3 cells towards neural compartment decreased as compared to the control with presence of neurites (Fig. S2A-C). We also introduced 6-OHDA in the neuronal compartment to induce neuron injury.[30] After incubation of 6-OHDA (100 µM) in neuronal channel for 1 h, the neurites were significantly destroyed (Fig. S2). However, owning to selectivity of 6-OHDA to neurons, incubation of 6-OHDA to PC-3 cells did not induce significant cytotoxicity to PC-3 cells *in vitro* (data not shown). After chemical ablation of DRG neurons by 6-OHDA, the neurotransmitters (including NE and ACh) released by DRG neurons were significantly decreased (Table S1). Without the presence of neurites and release of neurotransmitters, the migration of PC-3 cells was significantly inhibited (Fig. S2A-C). The surface area covered by migrated PC-3 cells was significant reduced after physical removal or chemical ablation of neurites in the interconnected region (Fig. S2D).

Time-lapse analysis of cancer cell migration

We analyzed the migration of individual PC-3 cell associated with neurites by time-lapse microscopy (Fig. 3), and we plotted the centroids of individual PC-3 cells to illustrate different modes of migration of PC-3 cells (Fig. 4). After peeling off the PDMS cover, the PC-3 cells disengaged from the cancer compartment, and migrated along the contacted neurites (Fig. 3A, Fig. 4A, Movie S1). The neurites provided a physical support for the migration of PC-3 cells toward the neuronal compartment (Fig. 3B, Fig. 4B, Movie S2). A few of PC-3 cells crossed between adjacent bundles of neurites for migration forward (Fig. 3C, Fig. 4C, Movie S3). The percentage of the crossing was 7.8 ± 3.1% by counting of 200 cells in time-lapse analysis. When the PC-3 cells arrived at the barrier of neuronal compartment, they may migrate backwards along the neurites (Fig. 3D, Fig. 4D, Movie S4). For the PC-3 cells which were not in contact with the neurites, the PC-3 cells exhibited random direction of migration (Fig. 3E, Fig. 4E, Movie S5). In contrast, without the presence of neurites in the interconnected regions, the spreading and migration of PC-3 cells was significantly inhibited (Fig. 3F, Fig. 4F, Movie S6).

Migration of individual cancer cell associated with neurites

We compared the migration of individual PC-3 cells with or without the contact with neurites (Fig. 5). The PC-3 cells along the contacted neurites exhibited an elongated and polarized morphology, with a shape index of 0.25 ± 0.06 (Fig. 5A, B). In contrast, the PC-3 cells without nerve contact showed less morphological changes with a shape index of 0.608 ± 0.111 (Fig. 5A, B). We measured the displacement (the distance between the start and end position, Fig. 5C), and divided it by the distance (that the cell travelled along its path, Fig. 5D), and

used their ratio to define the directionality of the cells (Fig. 5E). The results showed that PC-3 cells with nerve contact travelled longer distances with increased directivity, and reached a higher velocity of 0.86 ± 0.13 μm/min (Fig. 5C-G). In contrast, the PC-3 cells without nerve contacts exhibited random, non-directional movements and lower velocity (0.13 ± 0.11 μm/min) (Fig. 5C-G). Together, the PC-3 cells with nerve contact produced a single lamella in the leading edge (Fig. 5A), resulted in directionally persistent cell migration,[31] and increased migration rate of PC-3 cells (Fig. 5C-G). The PC-3 cells without nerve contacts produced multiple lamellae in PC-3 cells (Fig. 5A), resulted in random migration,[31] and decreased migration rate of PC-3 cells (Fig. 5C-G).

Migration of different cancer cells associated with neurites

We aimed to use the microfluidic co-culture system to examine the interaction of neurons with different types of cancers (Fig. S3). We selected different types of cancer cells (including PC-3 prostate cancer cells, Panc-1 pancreatic cancer cells, and MCF-7 breast cancer cells) based on clinical observation on their different rate of perineural invasion,[9] where prostate cancers and pancreatic cancers exhibit higher rate of PNI (75-80%, and up to 100%, respectively), but breast cancers exhibit a lower rate of PNI (3-38%).[9, 10] The on-chip result showed that PC-3 prostate cancer cells and Panc-1 pancreatic cancer cells exhibited greater migration along neurites than MCF-7 breast cancer cells from the cancer compartment toward the DRG neuronal compartment (Fig. S3A-B). The surface areas covered by the migrated PC-3 cells and Panc-1 cells were greater than that of MCF-7 cells (Fig. S3C). These results suggest that the migration of cancer cells along neurites was dependent on specific characteristics of cancer cells, and the results correlated with the clinical observations on PNI of different cancers.[9] The prostate cancers and pancreatic cancers exhibit higher rates of PNI,[9] and these cancer cells exhibited greater migration along neurites in the on-chip model, whereas the breast cancers exhibited a lower rate of PNI,[9] and the breast cancer cells exhibited a lower migration along neurites in the on-chip model.

The reasons for the preponderance of PNI in certain cancers (such as pancreatic cancer, head and neck cancer, prostate cancer) are not clearly understood,[3, 8, 9] but can be partially explained by the strong neurotrophic effects of these cancers and the close proximity to several neural plexuses. In turn, the abundance of innervations from neural plexuses generates an available interface for the migration and spreading of cancer cells via nerves.

Together, the above results showed that the neurites provided biophysical supports for the cancer cell attachment, guided and facilitated their migration (Fig. 2-5, Fig. S2). We found that the feature of cancer cell migration along neurites was a common phenomenon for different types of cancer cells, the cancers that have high levels of perineural invasion in clinical observations exhibited greater migration along neurites in the on-chip model (Fig. S3).

Neural-signaling-inhibitor regulates migration of cancer cells

We applied our on-chip model to achieve the screening of neural drugs which inhibit the migration of cancer cells along neurites. To do this, we aimed to target the most direct nerve-cancer signaling in prostate cancers with the on-chip model. For background introduction, prostate glands receive abundant innervations from sympathetic nervous system (SNS) and parasympathetic nervous system (PNS) (Fig. S4).[32, 33] SNS nerves release noradrenaline (NE), which binds to adrenergic receptors, whereas the PNS nerves release acetylcholine (ACh), which acts on muscarinic receptors on stroma cells of prostate.[33, 34] It is reported that the β-adrenergic receptors and muscarinic receptors are expressed by prostate cancer cells.[35, 36] The β-adrenergic signaling and ACh-muscarinic signaling are involved in the normal physiological function of prostates and prostate cancer development.[1, 35-37]

In the on-chip model, we confirmed the expression of neurotransmitters (NE and ACh) by DRG neurons by ELISA, the NE and ACh released by DRG neurons were determined to be 14.4 ± 2.9 nmol/L and 612 ± 69 nmol/L, respectively (Table S1). We also confirmed the expression of β-ARs (with β_1-AR and β_2-AR subtypes) and mAChRs (with m_1AChR and m_3AChR subtypes) on PC-3 cancer cells by western blot (WB) (Fig. S6). These results suggest that targeting nerve-cancer signaling by either NE-β-adrenergic signaling or ACh-muscarinic signaling may have potential in inhibiting cancer cell function (Fig. 6A).

In our on-chip model, we used non-selective β-blockers (including propranolol and penbutolol) to block the β-ARs on PC-3 cell surfaces, and we also applied non-selective muscarinic antagonists (atropine and hyoscine) to block the muscarinic receptors on PC-3 cells. These compounds are typically very safe and already applied in routine clinical practice.[38-40] After incubation of PC-3 cells with these compounds overnight, no significant cell cytotoxicity was observed from these compounds at lower concentration (≤ 10 μM) (Fig. S5). However, the treatment of β-blockers and muscarinic antagonists (at 10 μM for each agent) to PC-3 cells effectively down regulated the expression of β-adrenergic receptors and muscarinic receptors on PC-3 cells, respectively (Fig. S6).

On the chip-model, the blockade of NE-β-adrenergic signaling by β-blockers and the blockade of ACh-muscarinic signaling by muscarinic antagonists effectively inhibited the migration of PC-3 cancer cells along neurites (Fig. 6B,C). The surface area covered by migrated PC-3 cells in the interconnected region was significantly decreased after β-blockers and muscarinic antagonist treatment to PC-3 cells (Fig. 6D). Meanwhile, the use of agonist and antagonist on these signaling proved the sensitivity and specificity of the neuron-cancer crosstalk in the on-chip model (Fig. S7). These results suggested that blockage of nerve-cancer signaling impaired the migration of cancer cells along neurites (Fig. 6).

Discussion

Our microfluidic chip model provides a new method to study the interaction between neurons and cancer cells *in vitro* (Fig. 1). Using this on-chip model, we demonstrate that the neurites

provide biophysical support for the attachment of cancer cells, and guide their directional migration (Fig. 2-5). The cancers that have high levels of perineural invasion in clinical observations exhibit greater migration along neurites in the on-chip model (Fig. S3).

We then try to apply this on-chip model to investigate the signaling pathway between the neurons and cancer cells, to understand the neuronal cues that recruit cancer cells. Herein, we target the most direct nerve-cancer signaling pathway involving in prostate cancers, with NE-β-adrenergic signaling and ACh-muscarinic signaling, respectively (Fig. S4, Fig. 6A), since both signaling was involved in the physiological function of prostates and prostate cancer development.[1, 35-37] In the on-chip model, the inhibition of either NE-β-adrenergic signaling or ACh-muscarinic signaling effectively inhibited cancer cell migration along neurites (Fig. 6).

In the literature, the binding of NE to β-adrenergic receptors increases the intracellular level of cAMP (cyclic adenosine monophosphate), which activates PKA and PI3K pathway in cancer cells, resulting in the proliferation, progression and metastasis of cancers.[35] In our on-chip study, the blockade of NE-β-adrenergic signaling by β-blockers effectively decreases the cancer cell migration in the on-chip model (Fig. 6). Our on-chip results are consistent with previous studies that β-blocker inhibited NE-driven metastasis of prostate cancer cells in mice,[41] and β-blocker intake improved the survival of prostate cancer patients.[42]

Meanwhile, ACh-muscarinic receptor binding can activate PI3K signaling pathways in cancer cells, enhanced the cancer cell growth, proliferation and invasion of cancer cells.[36] Our on-chip results show that the blockade of ACh-muscarinic signaling by muscarinic antagonists also effectively reduced the cancer cell migration in the on-chip model (Fig. 6). Moreover, previous report shows the density of cholinergic fibers exceed that of adrenergic fibers in the overall prostate,[43] and our ELISA analysis showed a higher expression level of neurotransmitter (ACh) from cholinergic nerves (Table S1). The ELISA results support the applicability of on-chip assay as an *in vitro* model of the neural microenvironment.

In future work, our study will focus on the understanding of neuronal cues that recruit cancer cells, and investigating the associated nerve-cancer signaling pathway with the on-chip model. We will broaden the on-chip studies by application of the neurotrophic factors (such as nerve growth factor (NGF), brain-derived neurotrophic factor (BDNF), neurturin and artemin), migration associated protein (such as focal adhesion kinase (FAK)), or neuronal adhesion molecules (L1 cell adhesion molecule (L1CAM)) which are implicated in perineural invasion.

Conclusions

We successfully developed a high-throughput microfluidic chip-model to simulate the migration of cancer cells in the neural microenvironment. We used this chip to effectively screen the compounds for inhibition of cancer cell migration along neurites. With the on-chip model, we demonstrated that the neurites provided biophysical support for cancer cell attachment and facilitated the directional migration of cancer cells. The cancers that have high levels of perineural invasion in clinical observations exhibited greater migration along neurites in the on-chip model. The interruption of neurites, the blockade of nerve-cancer signaling inhibited cancer cell migration. Our on-chip model provides an excellent platform to investigate the dynamic interaction between cancers and neurons, which has great potential for investigations involving cancer tumor metastasis in the neural microenvironment.

Acknowledgements

We thank Professor Zhuan Zhou at Peking University for providing training for the culturing of DRG neurons. We thank Prof. Jane Y. Wu at Northwestern University for her original suggestion of using microfluidic devices to study cancer-neuron interactions. This work was supported by the MOST (2011CB933201, 2012AA030308), CAS (XDA09030305), CAS/SAFEA International Partnership Program for Creative Research Teams, NSFC (81361140345, 31470911). Y.F.L. is supported by China Postdoctoral Science Foundation (2014M550672) and the Scientific Research Foundation for the Returned Overseas Chinese Scholars, State Education Ministry.

Notes and references

1. C. Magnon, S. J. Hall, J. Lin, X. Xue, L. Gerber, S. J. Freedland and P. S. Frenette, Autonomic nerve development contributes to prostate cancer progression, *Science*, 2013, 341, 1236361.
2. C. M. Zhao, Y. Hayakawa, Y. Kodama, S. Muthupalani, C. B. Westphalen, G. T. Andersen, A. Flatberg, H. Johannessen, R. A. Friedman, B. W. Renz, A. K. Sandvik, V. Beisvag, H. Tomita, A. Hara, M. Quante, Z. Li, M. D. Gershon, K. Kaneko, J. G. Fox, T. C. Wang and D. Chen, Denervation suppresses gastric tumorigenesis, *Sci Transl Med*, 2014, 6, 250ra115.
3. C. S. Scanlon, R. Banerjee, R. C. Inglehart, M. Liu, N. Russo, A. Hariharan, E. A. van Tubergen, S. L. Corson, I. A. Asangani, C. M. Mistretta, A. M. Chinnaiyan and N. J. D'Silva, Galanin modulates the neural niche to favour perineural invasion in head and neck cancer, *Nat Commun*, 2015, 6, 6885.
4. S. C. Peterson, M. Eberl, A. N. Vagnozzi, A. Belkadi, N. A. Veniaminova, M. E. Verhaegen, C. K. Bichakjian, N. L. Ward, A. A. Dlugosz and S. Y. Wong, Basal cell carcinoma preferentially arises from stem cells within hair follicle and mechanosensory niches, *Cell Stem Cell*, 2015, 16, 400-412.
5. H. S. Venkatesh, T. B. Johung, V. Caretti, A. Noll, Y. J. Tang, S. Nagaraja, E. M. Gibson, C. W. Mount, J. Polepalli, S. S. Mitra, P. J. Woo, R. C. Malenka, H. Vogel, M. Bredel, P. Mallick and M. Monje, Neuronal Activity Promotes Glioma Growth through Neuroligin-3 Secretion, *Cell*, 2015, 161, 803-816.
6. J. C. Antoine and J. P. Camdessanche, Peripheral nervous system involvement in patients with cancer, *Lancet Neurol.*, 2007, 6, 75-86.
7. C. Liebig, G. Ayala, J. A. Wilks, D. H. Berger and D. Albo, Perineural invasion in cancer: a review of the literature, *Cancer*, 2009, 115, 3379-3391.
8. G. E. Ayala, H. Dai, M. Ittmann, R. Li, M. Powell, A. Frolov, T. M. Wheeler, T. C. Thompson and D. Rowley, Growth and survival

mechanisms associated with perineural invasion in prostate cancer, *Cancer Res.*, 2004, 64, 6082-6090.
9. A. A. Bapat, G. Hostetter, D. D. Von Hoff and H. Han, Perineural invasion and associated pain in pancreatic cancer, *Nat Rev Cancer*, 2011, 11, 695-707.
10. N. Maru, M. Ohori, M. W. Kattan, P. T. Scardino and T. M. Wheeler, Prognostic significance of the diameter of perineural invasion in radical prostatectomy specimens, *Human Pathology*, 2001, 32, 828-833.
11. K. Ondicova and B. Mravec, Role of nervous system in cancer aetiopathogenesis, *The Lancet. Oncology*, 2010, 11, 596-601.
12. M. Mancino, E. Ametller, P. Gascon and V. Almendro, The neuronal influence on tumor progression, *BBA-Rev Cancer*, 2011, 1816, 105-118.
13. G. E. Ayala, T. M. Wheeler, H. D. Shine, M. Schmelz, A. Frolov, S. Chakraborty and D. Rowley, In vitro dorsal root ganglia and human prostate cell line interaction: redefining perineural invasion in prostate cancer, *Prostate*, 2001, 49, 213-223.
14. G. M. Whitesides, The origins and the future of microfluidics, *Nature*, 2006, 442, 368-373.
15. Y. Li, B. Yuan, H. Ji, D. Han, S. Chen, F. Tian and X. Jiang, A method for patterning multiple types of cells by using electrochemical desorption of self-assembled monolayers within microfluidic channels, *Angew. Chem. Int. Ed.*, 2007, 46, 1094-1096.
16. Z. Chen, Y. Li, W. Liu, D. Zhang, Y. Zhao, B. Yuan and X. Jiang, Patterning mammalian cells for modeling three types of naturally occurring cell-cell interactions, *Angew. Chem. Int. Ed.*, 2009, 48, 8303-8305.
17. W. Liu, S. Xing, B. Yuan, W. Zheng and X. Jiang, Change of laminin density stimulates axon branching via growth cone myosin II-mediated adhesion, *Integr. Biol.*, 2013, 5, 1244-1252.
18. W. Liu, W. Zheng, B. Yuan and X. Jiang, A micropatterned coculture system for axon guidance reveals that Slit promotes axon fasciculation and regulates the expression of L1CAM, *Integr. Biol.*, 2013, 5, 617-623.
19. X. Mu, W. Zheng, J. Sun, W. Zhang and X. Jiang, Microfluidics for manipulating cells, *Small*, 2013, 9, 9-21.
20. A. M. Taylor, M. Blurton-Jones, S. W. Rhee, D. H. Cribbs, C. W. Cotman and N. L. Jeon, A microfluidic culture platform for CNS axonal injury, regeneration and transport, *Nat. Methods*, 2005, 2, 599-605.
21. Y. Li, M. Yang, Z. Huang, X. Chen, M. T. Maloney, L. Zhu, J. Liu, Y. Yang, S. Du, X. Jiang and J. Y. Wu, AxonQuant: A Microfluidic Chamber Culture-Coupled Algorithm That Allows High-Throughput Quantification of Axonal Damage, *Neurosignals*, 2014, 22, 14-29.
22. T. Sun, N. Yu, L.-K. Zhai, N. Li, C. Zhang, L. Zhou, Z. Huang, X.-Y. Jiang, Y. Shen and Z.-Y. Chen, c-Jun NH2-terminal Kinase (JNK)-interacting Protein-3 (JIP3) Regulates Neuronal Axon Elongation in a Kinesin- and JNK-dependent Manner, *J. Biol. Chem.*, 2013, 288, 14531-14543.
23. X.-Q. Chen, B. Wang, C. Wu, J. Pan, B. Yuan, Y.-Y. Su, X.-Y. Jiang, X. Zhang and L. Bao, Endosome-mediated retrograde axonal transport of P2X3 receptor signals in primary sensory neurons, *Cell Res.*, 2012, 22, 677-696.
24. Y. Y. Su, M. Ye, L. Li, C. Liu, J. Pan, W. W. Liu, Y. Jiang, X. Y. Jiang, X. Zhang, Y. Shu and L. Bao, KIF5B promotes the forward transport and axonal function of the voltage-gated sodium channel Nav1.8, *J. Neurosci.*, 2013, 33, 17884-17896.
25. K.-Y. Wu, M. He, Q.-Q. Hou, A.-L. Sheng, L. Yuan, F. Liu, W.-W. Liu, G. Li, X.-Y. Jiang and Z.-G. Luo, Semaphorin 3A activates the guanosine triphosphatase Rab5 to promote growth cone collapse and organize callosal axon projections, *Sci. Signal.*, 2014, 7, ra81-ra81.
26. Z. Huang, Y. Sun, W. Liu, W. Zhang, W. Zheng and X. Jiang, Assembly of Functional Three-Dimensional Neuronal Networks on a Microchip, *Small*, 2014, 10, 2530-2536.
27. Y. Liu, Y. Sun, H. Yan, X. Liu, W. Zhang, Z. Wang and X. Jiang, Electrospun fiber template for replica molding of microtopographical neural growth guidance, *Small*, 2012, 8, 676-681.
28. C. Zhang and Z. Zhou, Ca^{2+}-independent but voltage-dependent secretion in mammalian dorsal root ganglion neurons, *Nat. Neurosci.*, 2002, 5, 425-430.
29. Y. Lei, O. F. Zouani, M. Remy, C. Ayela and M. C. Durrieu, Geometrical microfeature cues for directing tubulogenesis of endothelial cells, *PLoS One*, 2012, 7, e41163.
30. R. M. Kostrzewa and D. M. Jacobowitz, Pharmacological actions of 6-hydroxydopamine, *Pharmacol Rev*, 1974, 26, 199-288.
31. R. J. Petrie, A. D. Doyle and K. M. Yamada, Random versus directionally persistent cell migration, *Nat Rev Mol Cell Bio*, 2009, 10, 538-549.
32. L. K. McCorry, Physiology of the autonomic nervous system, *American journal of pharmaceutical education*, 2007, 71, 78.
33. W. E. Farnsworth, Prostate stroma: physiology, *Prostate*, 1999, 38, 60-72.
34. S. Ventura, J. Pennefather and F. Mitchelson, Cholinergic innervation and function in the prostate gland, *Pharmacol. Ther.*, 2002, 94, 93-112.
35. S. W. Cole and A. K. Sood, Molecular pathways: beta-adrenergic signaling in cancer, *Clin Cancer Res*, 2012, 18, 1201-1206.
36. N. Shah, S. Khurana, K. Cheng and J. P. Raufman, Muscarinic receptors and ligands in cancer, *Am J Physiol Cell Physiol*, 2009, 296, C221-232.
37. S. W. Cole, A. S. Nagaraja, S. K. Lutgendorf, P. A. Green and A. K. Sood, Sympathetic nervous system regulation of the tumour microenvironment, *Nature Reviews Cancer*, 2015, 15, 563-572.
38. J. W. Black, A. F. Crowther, R. G. Shanks, L. H. Smith and A. C. Dornhorst, A new adrenergic: beta-receptor antagonist, *Lancet*, 1964, 283, 1080-1081.
39. B. G. Katzung, *Basic and Clinical Pharmacology (7th ed.)*, London: Appleton & Lange, 1998.
40. H. P. Rang, *Pharmacology*, Edinburgh: Churchill Livingstone., 2003.
41. D. Palm, K. Lang, B. Niggemann, T. L. t. Drell, K. Masur, K. S. Zaenker and F. Entschladen, The norepinephrine-driven metastasis development of PC-3 human prostate cancer cells in BALB/c nude mice is inhibited by beta-blockers, *Int J Cancer*, 2006, 118, 2744-2749.
42. H. H. Grytli, M. W. Fagerland, S. D. Fossa and K. A. Tasken, Association between use of beta-blockers and prostate cancer-specific survival: a cohort study of 3561 prostate cancer patients with high-risk or metastatic disease, *Eur Urol*, 2014, 65, 635-641.
43. L. P. Witte, C. R. Chapple, J. J. de la Rosette and M. C. Michel, Cholinergic innervation and muscarinic receptors in the human prostate, *Eur. Urol.*, 2008, 54, 326-334.

Figures and captions

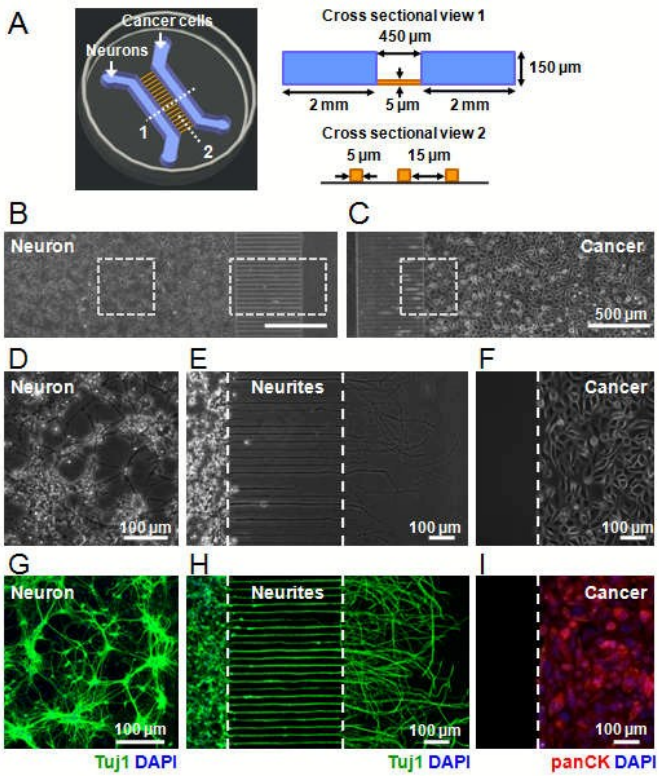

Fig. 1 Microfluidic chip for investigating the neuron-cancer cell interaction in vitro. (A) Schematic of a cell culture dish mounted with microfluidic compartmentalized device. The device is composed of two separate cell culture compartments (2 mm width, 150 μm height, 2 cm length), which are interconnected by an array of parallel microgrooves (5 μm width, 5 μm height, 450 μm length). (B-C) Phase-contrast images of the device seeded with either DRG neurons or cancer cells. (D, E, F) and (G, H, I) are magnified phase-contrast images (D, E, F) and fluorescent images (G, H, I) corresponding to the regions in (B-C). Neuron soma are confined in the neuronal channel (D, G), neurites grow and cross the interconnected microgrooves to reach the opposite compartment (E, H), whereas the cancer cells are limited in the cancer compartments (F, I). Neurons, cancer cells, and cell nuclei were stained with Tuj1 (green), panCK (red) and DAPI (blue), respectively. Dotted lines in the images indicated the borders of the two main compartmental channels.

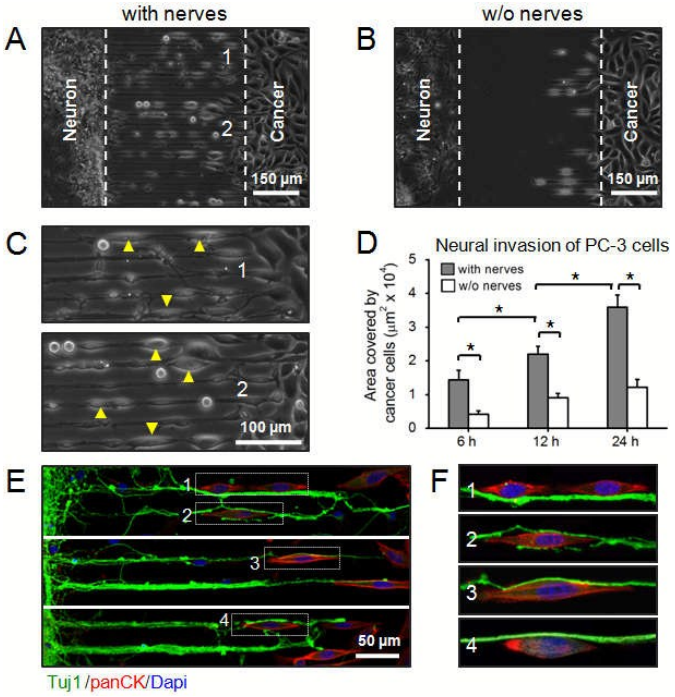

Fig. 2 Guided migration of PC-3 cancer cells with the presence of DRG neurites. (A) Representative phase-contrast images show the migration of the PC-3 cells with the presence of DRG neurites in the interconnected region at 24 h after removal of the PDMS cover. (B) The chips without the presence of neurites in the interconnected microgrooves served as control. (C) Magnified areas correspond to the regions indicated in (A), yellow arrowheads indicate the PC-3 cells navigating along the contacted neurites. (D) Quantification of the surface area covered by the migrated PC-3 cell projections in the interconnected regions at 6 h, 12 h, and 24 h after removal of PDMS covers. Data obtained from 10 random fields per sample, each counted field surface is 0.30 mm^2. * $p< 0.01$. (E) Immunofluorescent images of DRG neurons and PC-3 cells in the microfluidic chips. (F) Magnified images refer to the numbers indicated in (E). Neurons, cancer cells and nuclei are stained with Tuj1 (green), panCK (red) and DAPI (blue), respectively.

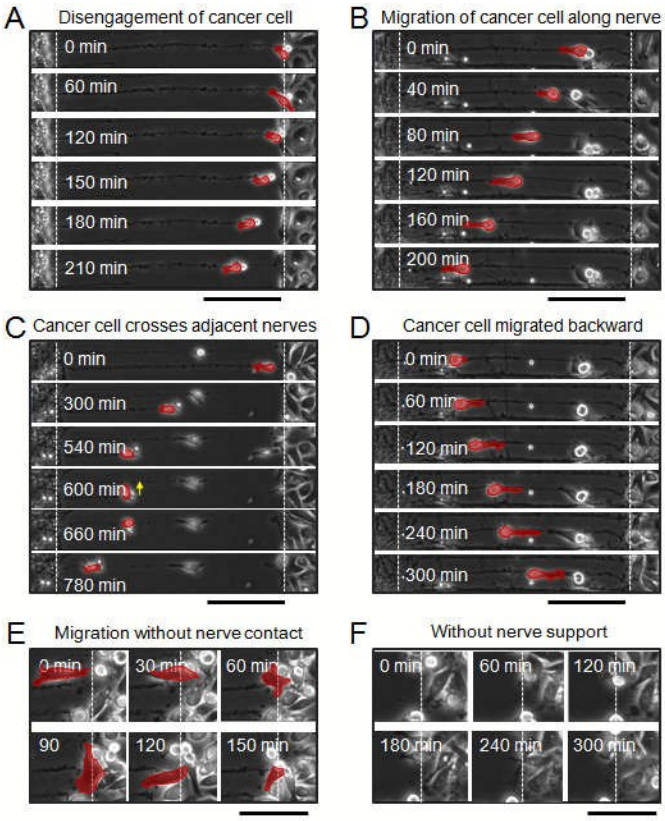

Fig. 3 Time-lapse images monitor the migration of PC-3 cells on the microfluidic chips. (A-D) Migration of individual PC-3 cell associated with the contacted neurites, (A) PC-3 cell disengages from the cancer compartment and migrates along the contacted neurites. (B) PC-3 cell navigates along the contacted neurites for migration forward. (C) Cancer cell navigates along the neurites and jumps to the adjacent neurites for migration forward. (D) Cancer cell migrates backward along the contacted neurites. (E) Migration of PC-3 cell which is not in contact with neurites. (F) Migration of cancer cells without the presence of neurites in the interconnnected regions. The tracked PC-3 cells are pseudo-colored in red. Scale bars, 150 μm in (A-D), and 50 μm in (E, F).

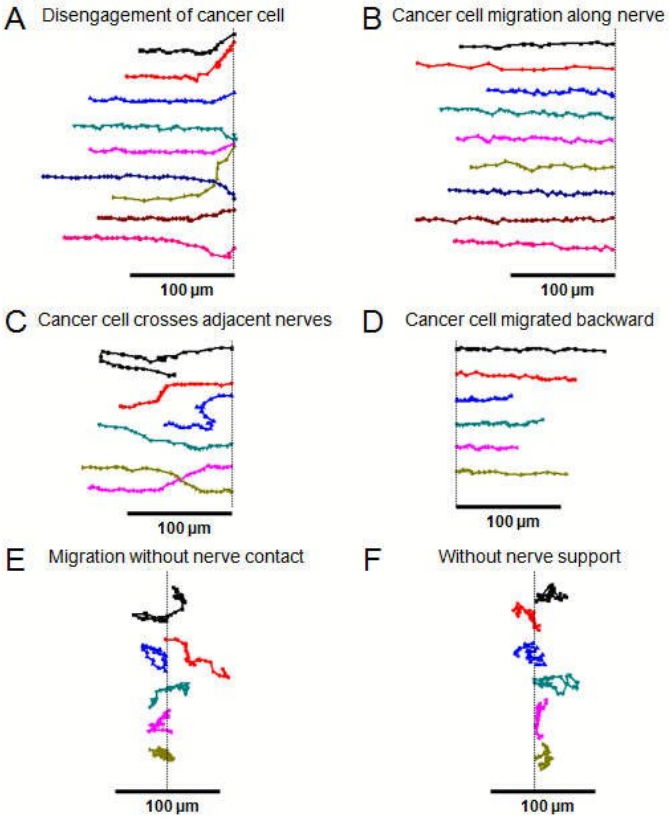

Fig. 4 Trajectory of PC-3 cells in the microfluidic chip model. The traces connect the positions of the centroids of cells at 3-h intervals, the traces are offset vertically along the dotted line for clarity. Each trace follows a separate cell. (A) PC-3 cell disengages from the cancer compartment and migrates along the contacted neurites. (B) PC-3 cell navigates along the contacted neurites for migration forward. (C) Cancer cell navigates along the neurites and jumps to the adjacent neurites for migration forward. (D) Cancer cell migrates backward along the contacted neurites. (E) Migration of PC-3 cell which is not in contact with neurites. (F) Migration of cancer cells without the presence of neurites in the interconnnected regions.

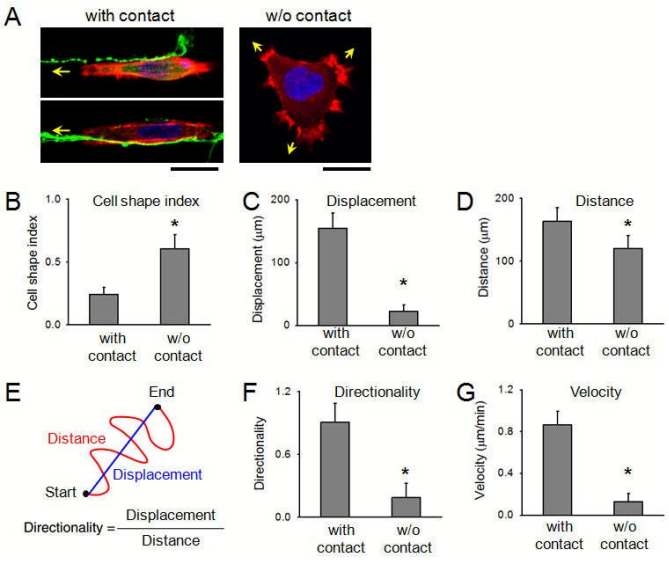

Fig. 5 Neurite contact enhances the directional migration of the PC-3 cells. (A-B) Representative confocal images of PC-3 cells migrating along the contacted neurites or without the contacted neurites. Neurons, PC-3 cells, and nuclei are stained by Tuj1 (green), phalloidin (red), and DAPI (blue), respectively. Yellow arrows indicate the direction of the migration of PC-3 cells. Scare bar, 20 μm. (B) Cell shape index, (C) Displacement, (D) Distance, (F) Directionality, and (G) Velocity of the PC-3 cells with or without the nerve contacts. *Cell shape index* is calculated according to the formula $I = 4\pi s/l^2$ (s: cell surface area, l: cell perimeter), cells are round as I being 1, and cells are infinitely elongated as I approaching 0. *Directionality* is defined as the displacement divided by the distance of the cell (E). If a cell is migrating more randomly, directionality decreases and vice versa. * $p < 0.01$.

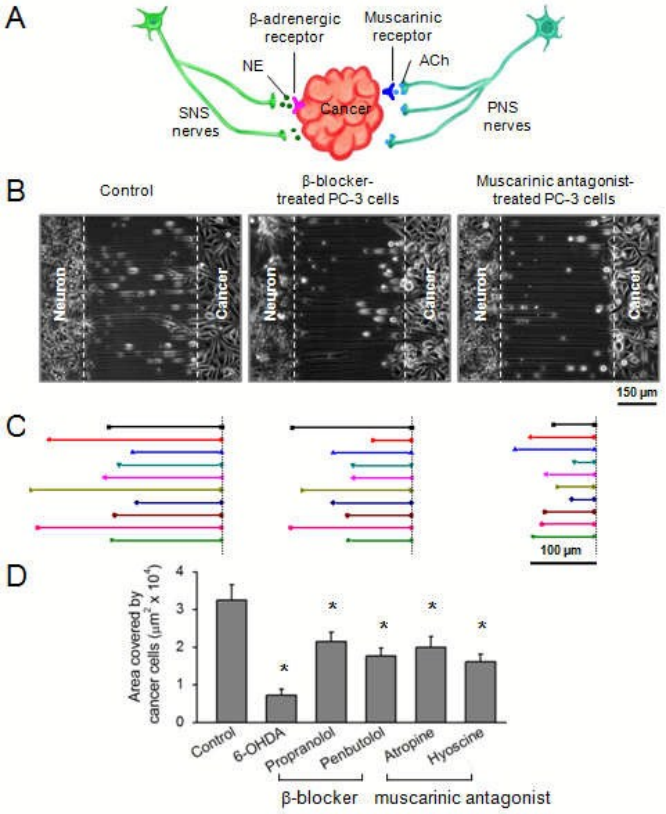

Fig. 6 Blocking the nerve-cancer crosstalk inhibits the migration of PC-3 cells along neurites. (A) Scheme of innervations of prostate cancers and relative nerve-cancer signaling. (B) Representative phase-contrast images show the migration of PC-3 cells at 24 h after peeling off PDMS covers, with no treatment to PC-3 cells as control group, or pre-treatment of PC-3 cells with β-blocker (propranolol, 10 μM), or with muscarinic antagonist (hyoscine, 10 μM). (C) Traces of PC-3 cells at 24 h intervals with treatment as indicated in (B). (D) Quantification of the surface areas covered by migrated PC-3 cells in the interconnected regions with different treatment at 24 h after peeling of the PDMS cover. Each counted field surface is 0.30 mm^2. * $p < 0.01$.

Graphical abstract

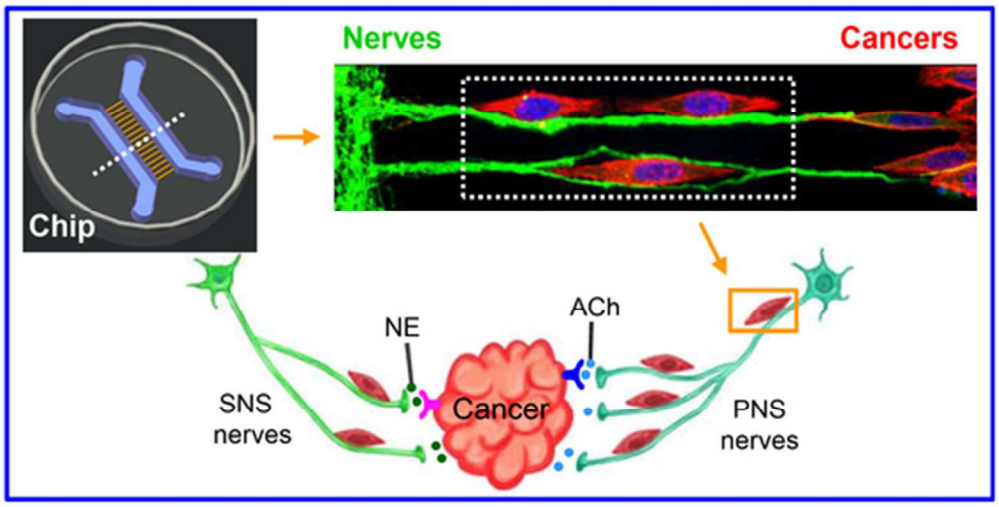

48x28mm (300 x 300 DPI)